Preliminary radiometric calibration assessment of ALOS AVNIR-2

Marc BOUVET,
European Space Agency
Wave Interaction & Propagation Section
Keplerlaan 1, PB 299
NL-2200 AG Noordwijk
The Netherlands
e-mail: marc.bouvet@esa.int

Philippe GORYL,
European Space Agency
Data Quality and Algorithms Office
Via Galileo Galilei
00044 Frascati (RM)
Italy
e-mail: philippe.gory@esa.int

Gyanesh CHANDER,
Science Applications International Corporation (SAIC),
USGS EROS
Sioux Falls, SD, 57198
USA
e-mail: gchander@usgs.gov

Richard SANTER,
ULCO
32, Avenue Foch.
F-629320 Wimereux
France
e-mail: santer@univ-littoral.fr

Sebastien SAUNIER
GAEL
Cite Descartes
25, rue Alfred Nobel
77420 Champs-sur-Marne
France
e-mail: sebastien.saunier@gael.fr

Abstract

This paper summarizes the activities carried out in the frame of the data quality activities of the Advanced Visible and Near Infrared Radiometer type 2 (AVNIR-2) sensor onboard the Advanced Land Observing Satellite (ALOS). Assessment of the radiometric calibration of the AVNIR-2 multi-spectral imager is achieved via three intercomparisons to currently flying sensors over the Libyan desert, during the first year of operation. All three methodologies indicate a slight underestimation of AVNIR-2 in band 1 by 4 to 7 % with respect to other sensors radiometric scale. Band 2 does not show any obvious bias. Results for band 3 are affected by saturation due to inappropriate gain setting. Two methodologies indicate no significant bias in band 4. Preliminary results indicate possible degradations of the AVNIR-2 channels, which, when modeled as an exponentially decreasing functions, have time constants of respectively 13.2 %.year^{-1}, 8.8 %.year^{-1} and 0.1 %.year^{-1} in band 1, 2 and 4 (with respect to the radiometric scale of the MEdium Resolution Imaging Spectrometer, MERIS). Longer time series of AVNIR-2 data are needed to draw final conclusions.

Keyword:ALOS, AVNIR-2, calibration, intercomparison, L5 TM, MERIS, POLDER-3, MODIS

I. INTRODUCTION

The Advanced Land Observing Satellite (ALOS) was launched on Jan 24th, 2006 onboard a JAXA H-IIA launcher. The planned operational lifetime is 3 years, in a near-polar, Sun-synchronous orbit, at a mean altitude of 691 km. Its payload consists of three sensors: Advanced Visible and Near Infrared Radiometer type 2 (AVNIR-2), Panchromatic Remote-sensing Instrument for Stereo Mapping (PRISM), Phased Array type L-band Synthetic Aperture Radar (PALSAR). The coverage and distribution of ALOS data is done through the implantation of the ALOS Data Node concept. The acquisitions performed globally are classified in four regions: Asia, Europe and Africa, America, Australia and Oceania (Figure 1). Each Data Node is responsible for the provision of level-1 data to the users within the geographical zone covered by the Node. In that framework, the ALOS Data European Node (ADEN) is run by the European Space Agency (ESA). ESA is supporting ALOS as a "Third Party Mission" which means that ESA uses its multi-mission ground systems of existing national and industrial facilities and expertise to acquire, process and distribute data. In that context, ESA-ADEN verified the ALOS data quality in order to get the approval for operating ALOS as Third party Mission and to report to JAXA on the product quality and calibration as member of the JAXA Cal/Val team.

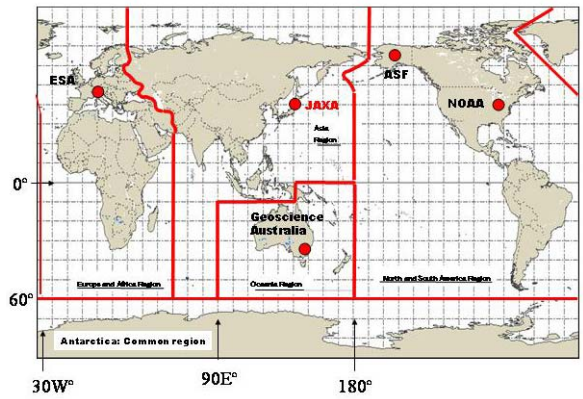

Figure 1: ALOS Data Nodes showing the various processing nodes.

In this frame, an assessment of the radiometric calibration of the AVNIR-2 instrument was carried out. The AVNIR-2 instrument onboard ALOS is a multispectral sensor operating in four spectral bands in the Visible and Near Infrared bands, with 10 m spatial resolution and a ground swath of 70 km at nadir. It has a pushbroom sensor with a radiometric quantization of 8 bits. The present paper is peculiar in its format since it is the compilation of three different approaches all aiming at assessing the radiometric calibration of AVNIR-2. All three approaches rely on comparisons with currently flying sensors. Intercomparison 1 is an intercomparison of or AVNIR-2 data and Landsat 5 (L5) Thematic Mapper (TM) data. Similarly, intercomparison 2 and 3 aim at positioning the AVNIR-2 radiometric calibration on the MERIS radiometric scale. All methodologies are applied to data acquired over the Libyan desert (see Figure 2) during 2006.

II. INTERCOMPARISON 1: ALOS AVNIR-2 DATA VS. LANDSAT 5 THEMATIC MAPPER DATA

Landsat 5 (L5) Thematic Mapper (TM) is an Earth-imaging sensor that was launched on March 1, 1984 with a design life on 3 years. It incorporated advancements in spectral, radiometric, and geometric capabilities relative to the Multispectral Scanner (MSS) flown on previous Landsat satellites. L5 TM Bands 1-5 and 7 have 16 detectors with center wavelengths of approximately 0.49, 0.56, 0.66, 0.83, 1.67, and 2.24 μm, respectively. The detectors for Bands 1-4 are located at the Primary Focal Plane (PFP), where the temperature is not controlled but normally varies between 292 and 300 K. The detectors for Bands 5, 6, and 7 are located at the Cold Focal Plane (CFP). The Internal Calibrator (IC) is incorporated as an onboard radiometric calibration system for the L5 TM. Onboard calibration of the TM uses lamps to calibrate the reflective bands and a blackbody source to calibrate the thermal band.

Figure 4 shows the RSR profiles between corresponding L5 TM and ALOS AVNIR-2 spectral bands. Table 1 summarizes the spectral of these sensors. The ALOS AVNIR-2 bands 1, 2, 3, and 4 are similar to the corresponding TM and ETM+ spectral bands

TABLE 1. SPECTRAL COVERAGE IN MM

Band	L5 TM	ALOS AVNIR-2
1	0.450-0.520	0.42-0.50
2	0.520-0.600	0.52-0.60
3	0.630-0.690	0.61-0.69
4	0.760-0.900	0.76-0.89
5	1.550-1.750	
6	10.40-12.50	
7	2.080-2.350	

A. Data

Due to the limited number of co-incident image pairs between these sensors, the scene selection for these studies proved to be a challenge. Due to the lack of near-simultaneous images available over the well-characterized and traditionally used calibration and application evaluation sites, alternate sites that have high reflectance, large dynamic range, high spatial uniformity, high Sun elevation, and minimal cloud cover were investigated. As a result, the final scenes selected for the current work were over Libya test site in Africa.

A cloud-free L5 TM scene was acquired on May 15, 2006, a day later on May 16, 2006 an ALOS AVNIR-2 scene covering part of the same footprint were acquired. Table 4 lists the scenes selected for the study, along with the scene ID number, the date and time of acquisition, and the Sun elevation angle for the scenes. Figure 2 shows the approximate image boundaries of the scenes used. The L5 TM scenes are referenced in the world reference system (WRS) 2 with path 181 and rows 040.

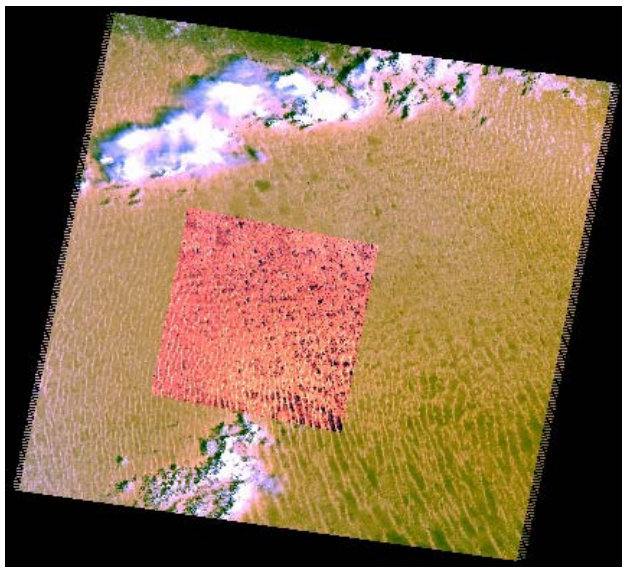

Figure 2. Image boundaries of scenes used in Libya collection

B. Methodology

Conversion from DN to absolute scale

Remote sensing satellite detectors exhibit linear response to incoming radiance, whether from the Earth's surface radiance or internal calibration sources. This response is quantized into 8-bit values that represent brightness values commonly called Digital Numbers (DN). To convert the calibrated digital numbers to at-aperture radiance, rescaling gains and biases are created from the known dynamic range limits of the instrument. Table 2 summarizes the rescaling gains and biases that are used for the DN-to-radiance conversion. For relatively "clear" scenes, a reduction in between-scene variability can be achieved through normalization for solar irradiance by converting the spectral radiance, as calculated above, to a planetary or exoatmospheric reflectance. When comparing images from different sensors, there are two advantages to using reflectance instead of radiances. First, the cosine effect of different solar zenith angles due to the time difference between data acquisitions can be removed, and second, it compensates for different values of the exoatmospheric solar irradiances arising from spectral band differences. Table 3 gives solar exoatmospheric spectral irradiances (ESUN) for the L5 TM and ALOS AVNIR-2 sensors.

TABLE 2: RESCLING GAINS AND BIASES USED FOR THE CONVERSION OF L1 CALIBRATED DIGITAL NUMNERS TO SPECTRAL RADIANCE FOR L5TM AND ALOS AVNIR-2

L5 TM		
Band	**$G_{rescale}$**	**$B_{rescale}$**
1	0.762824	-1.52
2	1.442510	-2.84
3	1.039880	-1.17
4	0.872588	-1.51
5	0.119882	-0.37
7	0.065294	-0.15

ALOS AVNIR-2	
$G_{rescale}$	**$B_{rescale}$**
0.941	0
0.914	0
0.804	0
0.835	0

TABLE 3 SOLAR EXOATMOSPHERIC SPECTRAL IRRADIANCES IN W/ (M^2. MM)

ESUN		
Bands	**L5**	**ALOS**
1	1957	1943.3
2	1826	1813.7
3	1554	1562.3
4	1036	1076.5
5	215	
7	80.67	

Calibration by near-simultaneous surface observations

Cross-calibration was performed with image statistics based on large common areas observed near-simultaneously by the two sensors. A feature simultaneously observed by these sensors is represented by slightly different numbers of image pixels because of the differences in viewing geometry and sensor scanning times. This makes it very difficult to establish sufficient geometric control to facilitate radiometric comparisons on a point-by-point and/or detector-by-detector basis. Therefore, the analysis approach made use of image statistics based on large homogenous areas common in the image pairs. Regions of Interest (ROI) were defined within these areas for each image. These large areas were carefully selected using distinct features common to both of the images. Both bright and dark regions were selected to obtain maximum coverage over each sensor's dynamic range, but areas with clouds or cloud shadows were excluded. ALOS AVNIR-2 band 3 images were mostly saturated as shown in Figure 3.

Figure 3. Saturation in ALOS AVNIR-2 Band 3. The red pixels are saturated pixels.

Once all area ROIs were selected, image statistics were computed to obtain mean and standard deviation target values on a band-by-band basis. The mean target statistics were then converted to absolute units of radiance and reflectance. Figure 5 shows the cross-calibration plots for the Libya collection. In each set of plots, the reflectance from the TM sensor is compared against the reflectance of the AVNIR-2 sensors for the six ROIs. Each data point on these plots represents an ensemble average of all pixels in a defined region for a given day and spectral band.

Figure 6 shows the reflectance comparison for each band. The plots on the right side represent average percentage differences in observation between the two sensors. The average percent differences in reflectance obtained from the ALOS AVNIR-2 relative to the L5 TM are summarized in Table IV. In band 1, the average percentage difference is -6.55%; in band 2, 1.24%; and in band 4, -4.99%.

One assumption made in the cross-calibration was that the at-sensor reflectance of all terrain in the study scenes underwent minimal changes between passes of the satellites. This may not be true for some regions of interest with changing wind conditions, and areas near clouds that may have had drastic changes in humidity between satellite passes. The transient changes due to aerosol loading between the two collections introduce uncertainty in the results. The relative spectral response (RSR) of the satellites is also a likely cause of error. Although measured in detail, prelaunch, spectral filters are known to degrade postlaunch and are difficult to characterize in orbit.

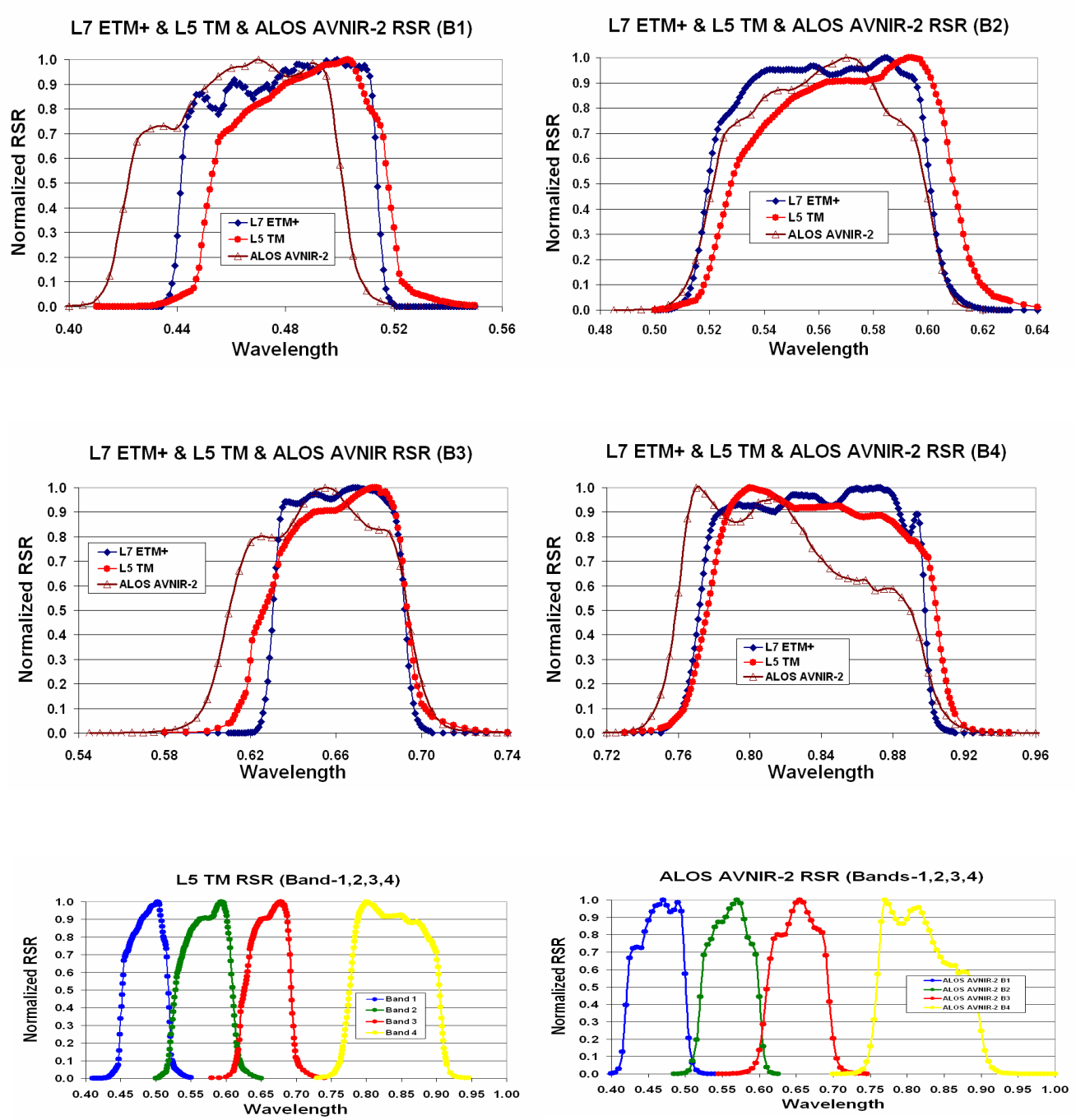

Figure 4. Relative Spectral Responses profiles of L5 TM and ALOS AVNIR-2 sensors

TABLE 4. COINCIDENT L5 TM AND ALOS AVNIR-2 SCENES USED FOR THIS STUDY

Sensor	Scene ID	Date	Time	Sun Elevation	Sun Azimuth	Pointing Angle
ALOS AVNIR-2	ALAV2A016383020	16-May-2006	9:10:12 AM	71.02°	116.88°	0°
L5 TM	LT5181040000613510	15-May-2006	8:47:16 AM	66.49°	109.53°	0°

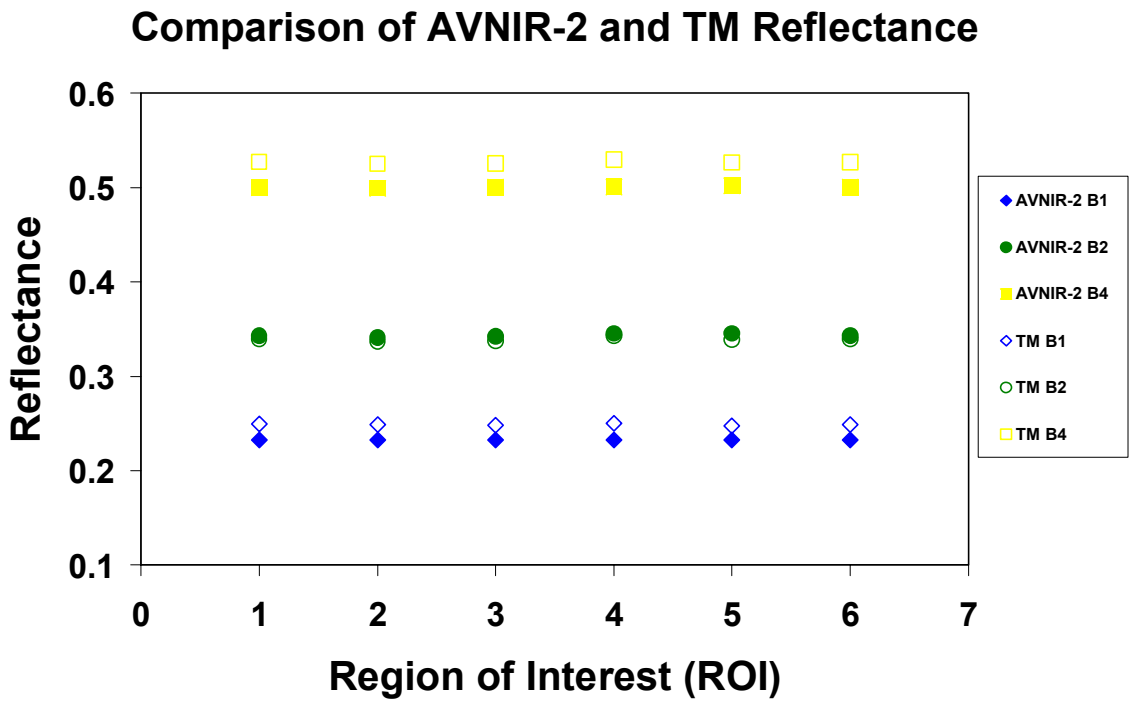

Figure 5: Reflectance of homogenous regions viewed by the TM and AVNIR-2 plotted for the six regions of interest (ROI)

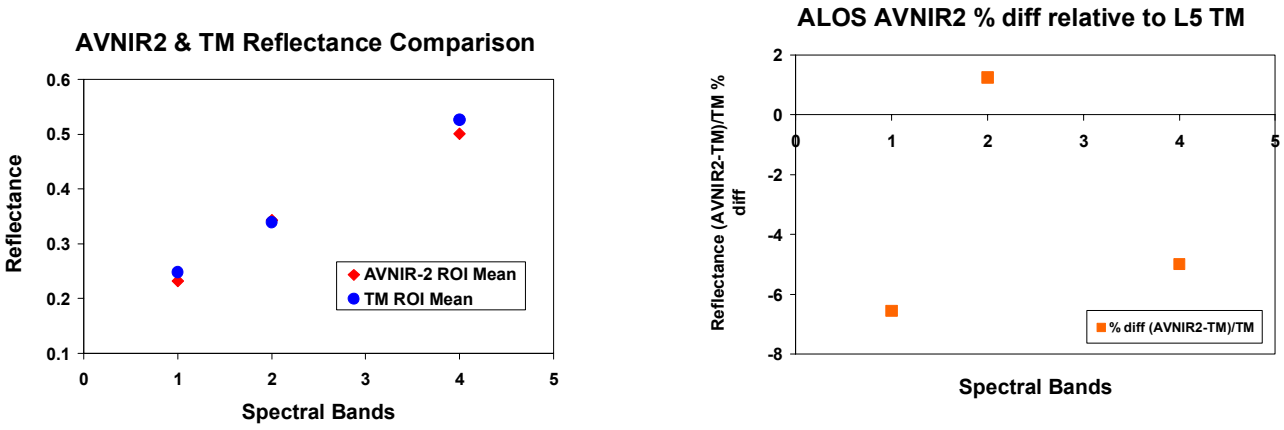

Figure 6: Comparison of the reflectance measurements from average of the six regions of interest (ROI) those were common to the bands 1, 2 and 4 of both the TM and AVNIR-2 sensors

III. INTERCOMPARISON 2: AVNIR-2 DATAS VS. SIMULATED AVNIR-2 DATA USING AATSR, A-MODIS, POLDER-3 AND MERIS DATA

This approach to the verification of the radiometric calibration of AVNIR-2 relies the intercomparison of the AVNIR-2 measurements in the four bands spanning from the UV to the NIR to simulations of the top-of-atmosphere (TOA) signal. The TOA signal simulations are obtained on the reconstruction of the TOA Bidirectional Reflectance Distribution Function (BRDF) of natural targets using multi-sensor observations, namely, POLarization and Directionality of Earth's Reflectances (POLDER-3), Aqua Moderate Resolution Imaging Spectroradiometer (MODIS) (A-MODIS), Advanced Along-Track Scanning Radiometer (AATSR) and Medium Resolution Imaging Spectrometer (MERIS).

A. Data

1) The multi-sensor dataset used for the simulation of the TOA signal in AVNIR-2 channels.

Data from four sensors acquired during 2006, over the western Libyan desert were acquired and visually cloud screen, then, they were converted to reflectance using the extraterrestrial spectrum in Figure 7 prior to be archived. These data are TOA calibrated and geo-referenced level 1b data:

- The AATSR data were generated by the L1b processor 5.59
- The A-MODIS data are extracted from the collection 5
- The MERIS data were generated with the prototype processor L1b MEGS PC 7.4 and the associated radiometric calibration
- The POLDER-3 data are generated from the L1b processor V2.02 and with the radiometric calibration V2.00

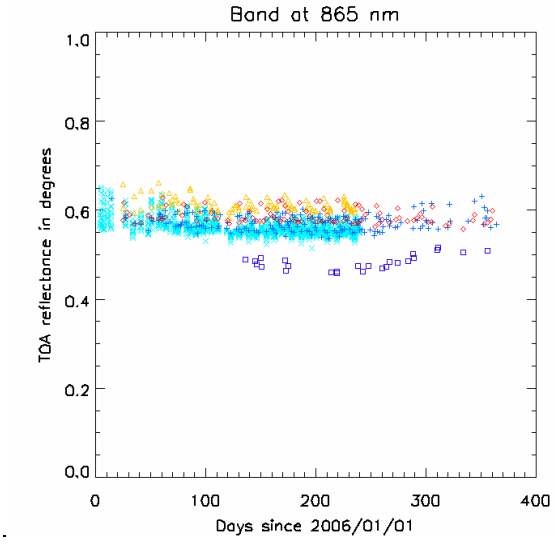

Figure 7. The L1b data time series of AATSR (orange triangles), A-MODIS (blue crosses), MERIS (red diamonds) and POLDER-3 (cyan crosses) over the Libyan desert, in 2006, in band 865 nm or equivalent. AVNIR2 L1b data in band 4 (blue square) are superimposed on this graph.

2) The AVNIR-2 data

Similarly, all data from AVNIR where extracted, cloud screened and converted to reflectances using the extraterrestrial solar irradiance from [4].

B. Methodology

AATSR, A-MODIS and POLDER-3 data were radiometrically rescaled to the MERIS data radiometric scale following a methodology described in [1]. In short, the principle of the radiometric rescaling to a reference sensor is the following:

1. For a given sensor and a given band, concomitant observations with the reference sensor (here MERIS) are identified, resulting in doublets of concomitant acquisitions (acquisitions are defined as concomitant if performed to within 1 day).
2. The geometries of observation and illumination of concomitant acquisitions are compared. Identical geometries (same angular positions of the sun and the two sensors with respect to the ground target) and reciprocal geometries (sun and sensor angular positions can be swapped) are identified.

Doublets of concomitant identical observations are considered directly comparable because the two sensors perform a same measurement concomitantly and under the same geometry. Assuming that the principle of reciprocity applies to the considered natural target surfaces, that is to say, that there are no shadowing effects, the reciprocal doublets can also be considered as being directly comparable.

From time series of such reciprocal and identical doublets, 2nd order polynomial are fit to the relative difference between a given sensor reflectance measurements and the equivalent reflectance measurement in the appropriate band of the reference sensor. A discussion on the impact of the differences between sensor relative spectral responses and applicability of the reciprocal principle can be found in [1]

Using these polynomials, all acquisitions from AATSR, A-MODIS and POLDER-3 (including those which are not part of a doublet of identical or reciprocal) are radiometrically rescaled to the MERIS radiometric scale. Such processing results into a radiometrically homogeneous dataset of AATSR, A-MODIS, POLDER-3 and MERIS data (see Figure 8). Hereafter, this ensemble of level 1b data radiometrically consistent originating from the 4 sensors is referred to as the homogeneous dataset. The homogeneous dataset is constituted of measurements in the following bands: 443 nm, 490 nm, 560 nm, 670 nm and 865 nm.

The homogeneous dataset is used to invert a spectral BRDF model of the target. Such BRDF model is based on the linear model driven by 3 kernel function and is described in [2]. The inversion of the BRDF is carried out on a 5-day basis. Such BRDF model can be use to predict the TOA reflectance for a given geometry of illumination or observation in the narrow bands at 443 nm, 490 nm, 560 nm, 670 nm and 865 nm.

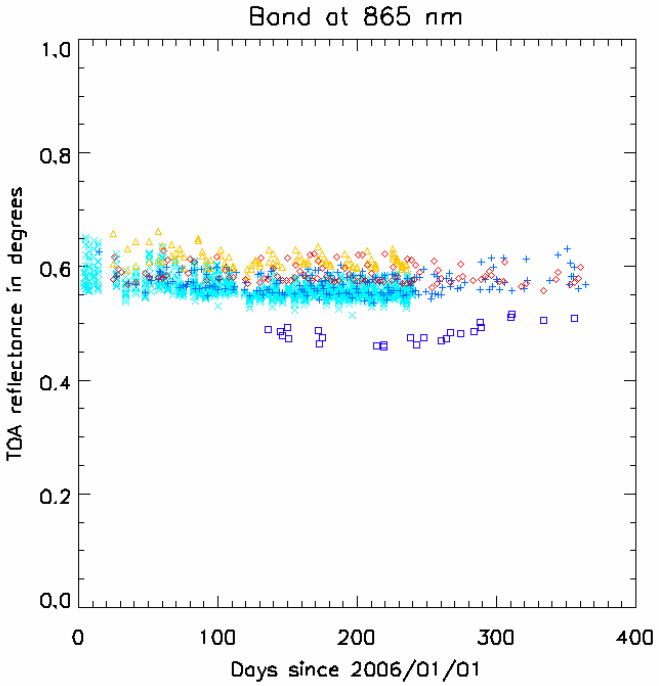

Figure 8. The L1b homogenous data time series derived from AATSR, A-MODIS, POLDER-3 and MERIS. The homogeneous dataset is a radiometrically homogeneous data referenced to the MERIS radiometric scale originating from AATSR (orange triangles), A-MODIS (blue crosses), MERIS (red diamonds) and POLDER-3 (cyan crosses). Theses data were acquired over the Libyan desert, in 2006, in band 865 nm. The AVNIR2 L1b data in band 4 (blue square) which radiometric characteristics are superimposed on this graph

The final objective of the methodology is to simulate AVNIR-2 TOA reflectances. But the AVNIR-2 measurements are performed in 4 bands that are broader that the 10 to 20 nm wide bands of AATSR, A-MODIS, MERIS and POLDER-3. To simulate the TOA reflectance in AVNIR-2 bands for a given day, the 5-day narrow band BRDFs are used to simulated narrow band TOA reflectances. Subsequently, 5-day full TOA reflectance spectra are reconstructed by linear interpolation between the simulated narrow band reflectances.

Simulated AVNIR-2 reflectance can be obtained by convolution of the 5-day simulated spectra with the relative spectral response of AVNIR-2 (see Figure 9). Such simulated AVNIR-2 reflectances are however not completely representative of the actual AVNIR-2 measurements although both the spectral and directional properties of the target have been taken into account. Indeed, because the AVNIR-2 bands extend over spectral region where the gaseous absorption is significant, the measured reflectances differ from the ones simulated using the homogeneous dataset. The narrow bands of the homogeneous dataset are almost unaffected by water vapour absorption and dioxygen absorption. Conversely, the AVNIR-2 bands 3 and 4 are significantly affected by absorption from the two gases. The influence of absorption on the AVNIR-2 data is illustrated in Figure 9.

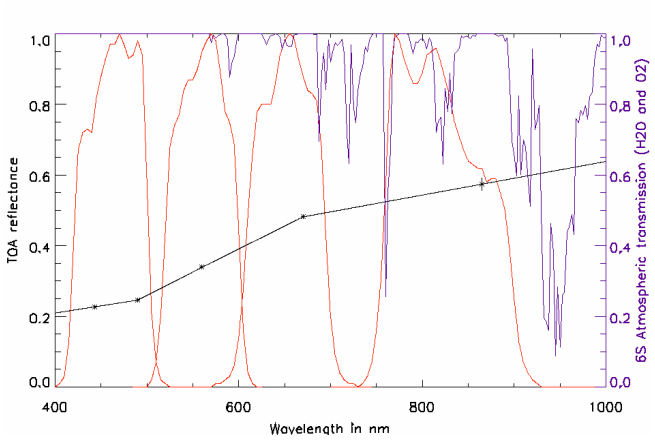

Figure 9. This figure shows the 5-day spectrum (black line) obtained from linear interpolation beetween the 5-day narrow band TOA reflectances of the homogeneous dataset (black stars). Supperimposed, in red, the relative spectral response of AVNIR-2 in its 4 bands from which the AVNIR-2 reflectance are simulated. and the 6S gaseous transmission of O_2 and water vapour (2.14 g/cm). Thes are the 5-day spectrum and the transmission corresponding to the AVNIR-2 acquistion of the day of the year 136 of 2006.

Concerning the influence of ozone, it is here assumed that the influence of ozone is relatively well mapped by the 5-day simulated spectra based as the spectral sampling of the narrow bands of the homogeneous dataset is sufficient to follow the spectral variations of the absorption induced by ozone (see Figure 9).

To fully simulate the AVNIR-2 measurements from the 5-day spectra, a correction for O_2 and H_2O is applied by computing the gaseous transmission of these gases, in the AVNIR-2 bands, along the downwelling and upwelling optical path. Such direct transmission computation in the 4 AVNIR-2 bands, for each AVNIR-2 acquisition is computed with 6S [3]. Using the direct transmission along the optical path to correct for the absorption is not rigorous when multiple scattering occurs. However, because these gaseous absorption corrections are significant only in AVNIR band 3 and 4 where important surface brightness induces that the single scattering of photons at the surface is predominant in the TOA signal, the assumption of a gaseous transmission reducing to the direct transmission can be justified.

O_2 absorption is driven by pressure and temperature profiles. Both are considered constant (mid-latitude summer profile) for each AVNIR-2 acquisition.

Water vapour data were obtained from the Aqua-MODIS level 3 daily atmospheric products. The total columnar water-vapor MODIS level 2 product from which the daily level 3 product are derived is claimed to have an accuracy of 5-10% (http://modis-atmos.gsfc.nasa.gov).

C. Discussion

In the attempt to reproduce AVNIR-2 measurements from AATSR, A-MODIS and POLDER-3 data rescaled to the MERIS radiometric scale several errors are introduced.

Errors on the inversion of the BRDF

Once the data from the AATSR, A-MODIS and POLDER-3 have been rescaled to the MERIS radiometric scale using the identical and reciprocal doublets, they are concatenated into the so-called homogeneous dataset which in turn, is used to fit a 5-day BRDF model in each band. The quality of the fit of the 5-day BRDF model to the homogenous dataset is illustrated in Figure 10 where a total 51 homogeneous TOA reflectances originating from AATSR, A-MODIS, MERIS and POLDER-3 acquisitions are mapped against the BRDF model predictions. The RMSE between the homogeneous data and the BRDF model is 1.24 % for this particular 5-day bin.

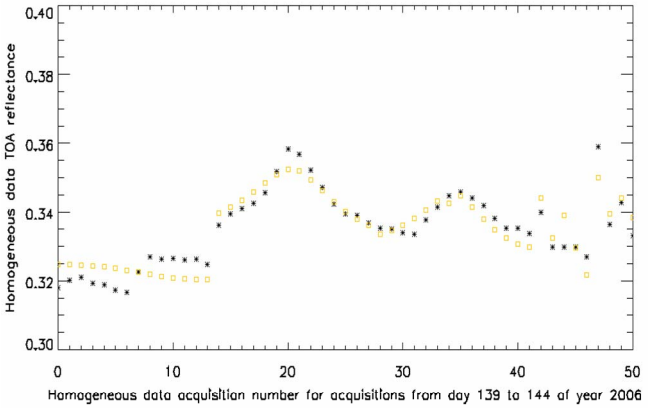

Figure 10. All homogeneous data over the Lybian desert at 560 nm : 42 POLDER-3 acquisitions followed by 4 AATSR acquistions , 3 A-MODIS acquisitions and 2 MERIS acquisitions are represented as orange squares. For the multiview intruments POLDER-3 and AATSR, each viewing geometry is considered as a separate acquisition. Superimposed, the TOA reflectances derived from each acquisition viewing / illumination geometry and the 5-day BRDF model (black stars). The RMSE between the homogeneous dataset and the BRDF model predictions is 1.24 %

Similarly, for each 5-day bin, in 2006, the RMSE associated to the 5-day BRDF model inversion is derived. This is shown in Figure 11.

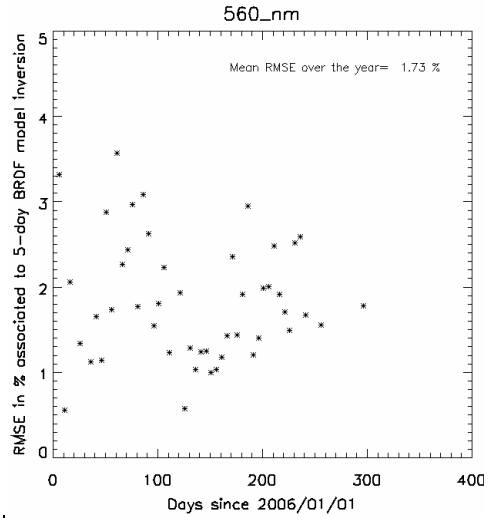

Figure 11. RMSE associated to the inversion of the 5-day BRDF model at 560 nm for each 5-day bin.

Table 5 indicates the RMSE, between the homogeneous dataset and the predictions of the 5-day BRDF model averaged over 2006, in each narrow band.

TABLE 5. THE RMSE OF THE HE 5-DAY BRDF MODEL INVERSION AVERAGED OVER 2006

Wavelength in nm	RMSE in % between BRDF model data and homogeneous dataset
443	2.99
490	2.06
560	1.73
670	1.31
865	1.86

The results of Table 5 can be interpreted as the capability of the BRDF model to generate 5-day TOA reflectance spectra on the radiometric scale of MERIS, in narrow bands, with an accuracy of 2-3 % RMSE. To estimate the uncertainty associated to the final simulated AVNIR-2 in band reflectance (which is here the reference against which actual AVNIR-2 measurements are assessed), the error on the correction of absorption of water vapour and dioxygen should also be taken into account.

Moreover, the linear interpolation of the narrow band 5-day spectra prior to convolution with the AVNIR-2 relative spectral response is also an approximation introducing errors difficult to quantify.

Errors on the gaseous absorption transmission

Assuming that the assumption of single scattering in band 3 and band 4 of AVNIR-2 and exact computation of the direct gaseous transmission on the upwelling and downwelling optical path, the residual error in the gaseous absorption correction is due to uncertainties in MODIS level 3 daily product which is about 10 % as previous mentioned.

Table 6 shows the mean difference obtained for all AVNIR-2 acquisitions between the TOA reflectances measured by the instrument and those simulated by the previously described methodology. This Table 6 shows that the impact of the uncertainty on the total columnar water vapour is less than half a percent on the simulated TOA reflectances. The correction is however significant: about 1.5 % in band 2 and 3 and up to 7 % in band 4.

If we quadratically sum up the RMSE of the 5-day BRDF inversion and the water vapour uncertainty we end up with an uncertainty on the simulated AVNIR-2 TOA reflectance of about 3 %. This uncertainty does not include the errors due to the fact that the 5-day TOA spectra are the result of the linear interpolation of only 5 narrow band TOA reflectances (443 nm, 490 nm, 560 nm, 670 nm and 865 nm). This should further degrade the accuracy of the methodology to about 5 %.

TABLE 6. THE MEAN DIFFERENCE BETWEEN THE AVNIR-2 TOA REFLCETANCE AND THE SIMULATED AVNIR-2 TOA REFLECTANCES FOR 3 GASEOUS ABSORPTION CORRECTIONS. IN THE TALBE WV STANDS FOR WATER VAPOUR.

	Without WV correction	With WV correction	With WV correction and 10 % error on WV
Mean difference for Band 1 (in %)	-7.0	-7.0	-7.0
Mean difference for Band 2 (in %)	-2.3	-1.1	-1.0
Mean difference for Band 3 (in %)	-3.9	-2.5	-2.3
Mean difference for Band 4 (in %)	-10.3	-3.5	-3.1

Saturation in AVNIR-2 band 3

When interpreting the results here presented, it should be borne in mind that the radiometric gains of the AVNIR-2 in band 3 were unfortunately set in such way that there is a residual saturation over the Libyan desert. Such saturation occurs for most acquisitions, and in a number of cases at the peak of the distribution of reflectances within the region of interest. When using average values over such region of interested, as done in this study, such saturation results into underestimates of the actual mean reflectance over the region of interest.

D. Results

Figure 12 is a comparison between the simulated AVNIR-2 measurements and the actual AVNIR-2 measurement. The dynamic range induced by the variations of reflectance measured over the Libyan desertic site is not sufficient to draw conclusion on the linearity of the AVNIR-2 instrument response with respect to the homogeneous dataset.

Figure 13 shows the ratio of the actual AVNIR-2 TOA reflectances to the simulated TOA reflectances plotted against time. This enables inverting parameters of the two-parameter degradation model reading as follow for each band:

$$\frac{\rho_{AVNIR2}}{\rho_{AVNIR2}^{simulated}}(t) = \frac{\rho_{AVNIR2}}{\rho_{AVNIR2}^{simulated}}(t = 01/01/2006) \times \exp(-\tau.t)$$

Table 7 summarizes these results.

About the temporal variation of the TOA reflectances over the Libyan desert site.

TOA reflectances, for all sensors AATSR, POLDER-3, MODIS, MERIS and AVNIR-2, in all bands from the UV to the NIR, over the Libyan desert, show a seasonal variation. In winter, TOA reflectances, for a given band, are higher than in summer. Our dataset of simulated AVNIR-2 data only extend over about 4 month. The degradation trends presented in Table 7 are thus to be confirmed over a period of at least a year. The degradation here measured over 4 months could be an artifact du to the seasonal variation in the TOA signal.

TABLE 7. `THE COMPARISON OF AVNIR-2 TOA REFLECTANCES AND THE SIMULATED AVNIR-2 REFLECTANCES. THE INTERPRETABILITY OF RESULTS FOR BAND 3 SUFFER FROM THE SATURATION OCCURING IN THIS BAND

	Mean relative difference with simulated TOA reflectances (in %)	Standard deviation to the mean (in %)	Degradation in %.year-1
Band 1	-7.0	1.7	13.2
Band 2	-1.1	1.4	8.8
Band 3	-2.5	2.0	5.9
Band 4	-3.5	1.4	0.1

The error budget of the methodology is estimated to about 5 %. AVNIR-2 appears to be 7.0 %, 1.1 %, 2.5 % (saturated band) and 3.5 % bellow the radiometric scale of MERIS in respectively band 1, 2, 3 and 4. Band 3 suffers from saturation and the results for this specific band are too difficult to interpret. All AVNIR-2 bands but band 1 are within this error budget.

Degradation appears to be detected in each band. When modeled as an exponentially decrease, the time constants are respectively 13.2 %.year-1, 8.8 %.year-1, 5.9 %.year-1 and 0.1.year-1 % in band 1, 2, 3 and 4 (with respect to the radiometric scale of MERIS). The degradation figures can however only be confirmed after one full year of AVNIR-2 data over the Libyan site have been processed to ensure that such degradation is not an artifact induced by the methodology itself.

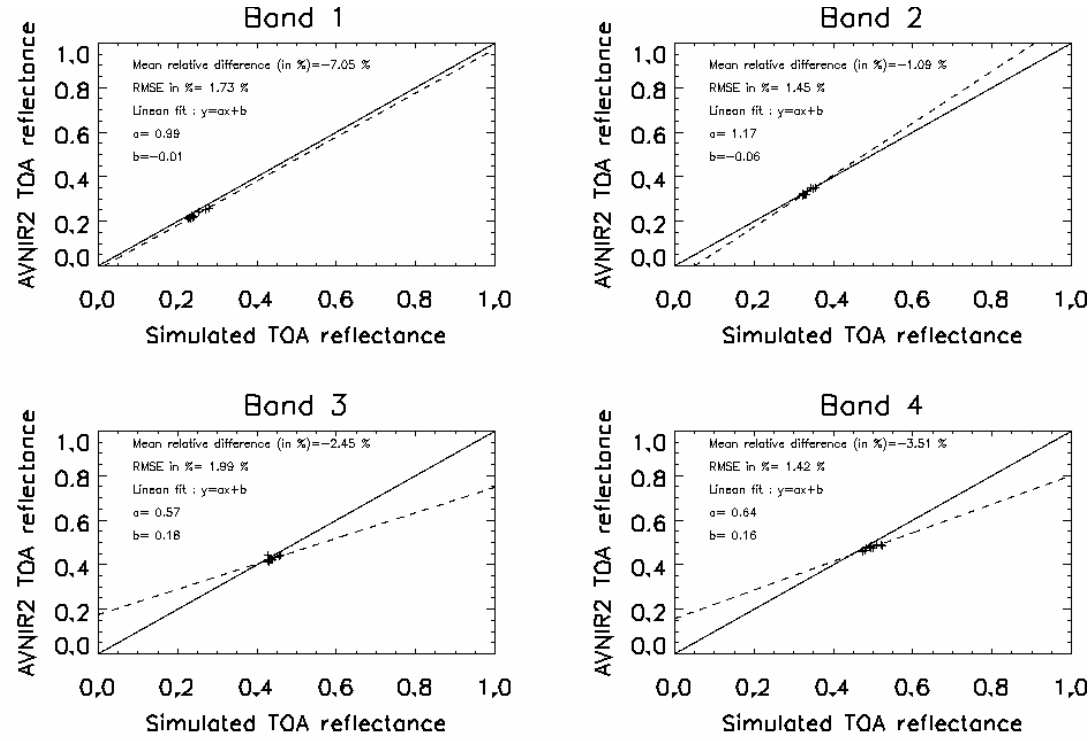

Figure 12. Comparison between the AVNIR-2 TOA reflectances over the Lybian desert, in 2006, in band 1, 2, 3 and 4 and the corresponding simulated TOA reflectances.

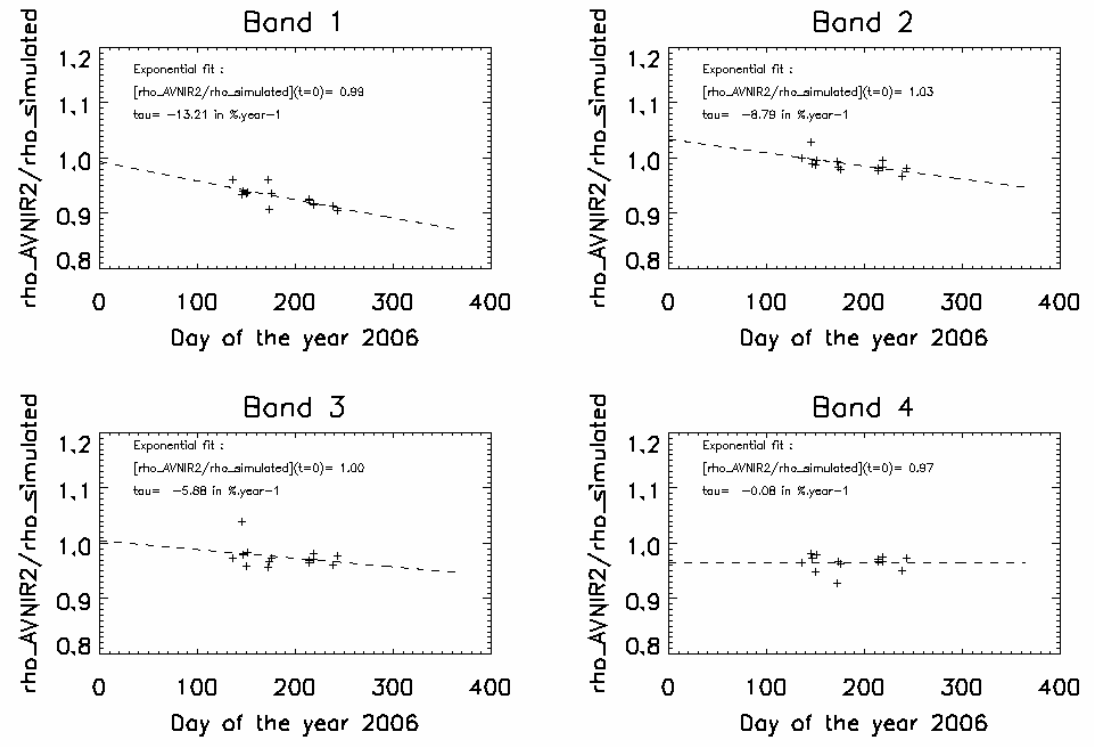

Figure 13. The temporal evolution of the ratio of AVNIR-2 TOA reflectance over the simulated TOA reflectance. As indications, the coefficient of the exponential fit of the ratio are also given on each figure.

IV. INTERCOMPARISON 3:AVNIR-2 DATA VS. SIMULATED AVNIR-2 DATA USING MERIS DATA

The objective of this intercomparison is to simulate the AVNIR-2 TOA reflectance using MERIS data over the Lybian desert.

A. Data

The MERIS and AVNIR-2 L1b datasets used in this second intercomparison are identical to those described in the previous intercomparison.

B. Methodology

The methodology is based in the identification of the linear relationship between the TOA reflectance and the scattering angle. To illustrate this BRDF effect, Figure 14 shows the temporal variation of the TOA reflectance of MERIS in 3 bands. Figure 15 shows the same TOA reflectance dataset ordered by increasing scattering angle and highlights its linear dependence.

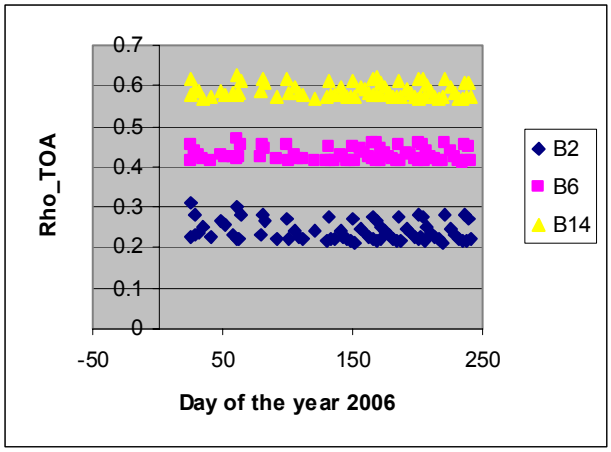

Figure 14. The temporal variation of the MERIS TOA reflectances in band 2 (443 nm), 3 (490 nm) and 14 (885 nm)

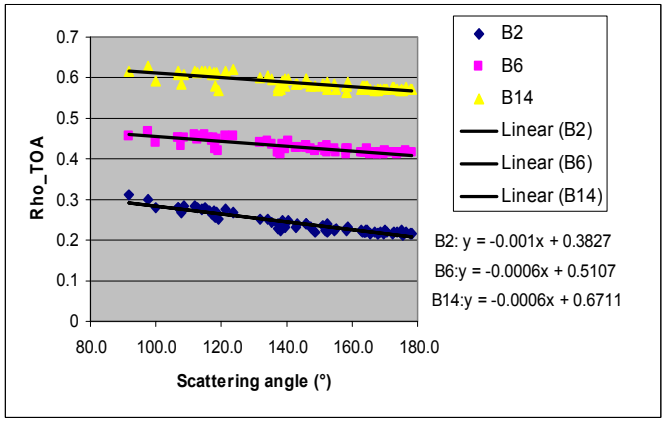

Figure 15. The variations of the MERIS TOA reflectance with respect to the scattering angle

Figure 16 shows the linear behavior of the BRDF with respect to the scattering angles in the case of the AVNIR-2 data. Such linear behavior appears noisier than using the MERIS TOA reflectance. The BRDF model defined hereafter is thus based on the MERIS data.

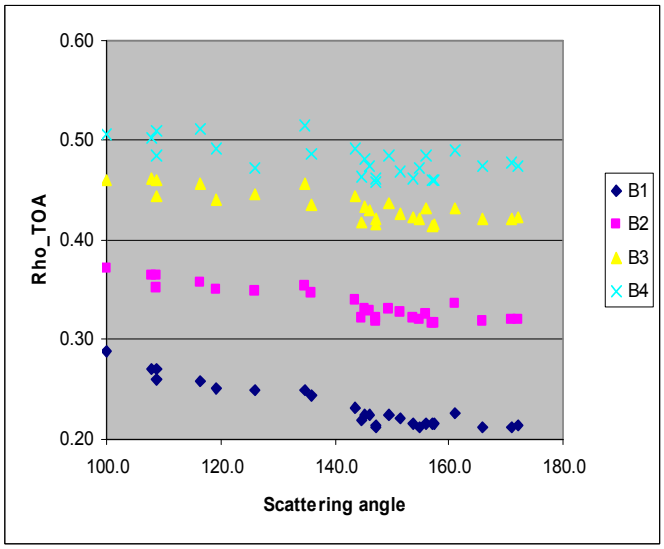

Figure 16. The variation of the AVNIR-2 TOA reflectances with the scattering angle

Effective wavelength

In order to compare the spectral characteristics of two instruments, we introduce the effective wavelength:

$$\lambda^k = \frac{\int_0^\infty \lambda S_k(\lambda) E_S(\lambda) d\lambda}{\int_0^\infty E_s(\lambda) S_k(\lambda) d\lambda}$$

For MERIS, the band widths are narrow enough to use the nominal central wavelengths as effective wavelengths. For AVNIR-2, we use the previous equation to produce Table 8.

TABLE 8. EFFECTIVE WAVELENGTHS FOR AVNIR-2

band	B1	B2	B3	B4
λ(nm)	465	560	652	819

Using the spectral information in Table 8, the simulation of AVNIR-2 data from MERIS data can done by computing the TOA reflectance at the effective wavelength in the following way:

- B1-AVNIR-2: linear interpolation between B2-MERIS (443 nm) and B3_MERIS (490nm)
- B2_AVNIR-2 equals B5_MERIS (560 nm)
- B3-AVNIR-2: linear interpolation between B6-MERIS (620 nm) and B7_MERIS (665 nm)

- B4-AVNIR-2: linear interpolation between B12-MERIS (779 nm) and B13_MERIS (865 nm)

Using the previous correspondences, the MERIS dataset is turned into an AVNIR-2 like dataset for the MERIS geometries of observation. This is shown in Figure 17.

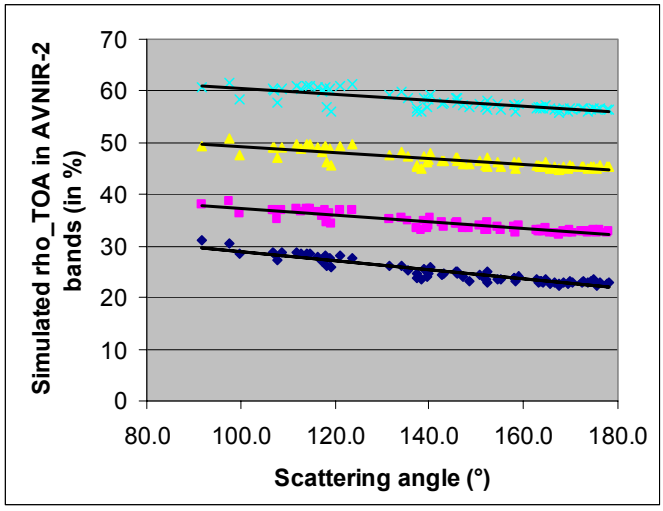

Figure 17. The simulated AVNIR-2 data using the MERIS data.

Retrieving the BRDF spectral model for AVNIR-2 bands

The linear fit of the simulated AVNIR-2 data provides linear BRDF models for each AVNIR-2 spectral band. The corresponding parameters are reported in Table 9.

TABLE 9. THE COEFFICIENTS OF THE LINEAR FIT OF THE BRDF FROM THE SIMULATED AVNIR-2 DATA DERIVED FROM MERIS DATA.

	slope	intercept	R2
B1	-0.000895	0.3790	0.8912
B2	-0.000653	0.4372	0.8336
B3	-0.000587	0.5515	0.7292
B4	-0.000581	0.6631	0.6540

Reconstruction of the AVNIR-2 data from the BRDF model

Using the previously obtained BRDF model for the AVNIR-2 spectral bands, the TOA reflectance in AVNIR-2 geometries of observation can be simulated. In turn, these simulated AVNIR-2 reflectance can be compared to the actual AVNIR-2 TOA reflectances.

Comparison of the AVNIR-2 data and the simulated AVNIR-2 data

Table 10 gives the simple ratio between the AVNIR-2 TOA reflectance and the simulated AVNIR-2 reflectance based on the MERIS data.

Gaseous absorption

It is assumed here that the most significant effects of absorption are caused by water vapour absorption and that the most affected band is the AVNIR-2 band 4. Using the results from the previous intercomparison as approximations of the gaseous absorption we can anticipate increases of respectively about 1.2 %, 1.4% and 6.8% in band 2, 3 and 4. These absorption values are averaged values derived for the AVNIR-2 dataset used in intercomparison 2. This AVNIR-2 dataset slightly differs from the dataset here, however, these mean absorption values should be good approximations for intercomparison 3. When applied to the simulated AVNIR-2 data, these absorption values result into differences between actual data and simulated data derived from MERIS, in band 1, 2, 3 and 4 of respectively -4.6 %, -1.4%, -5.9% and -10.3%.

TABLE 10. RATIO OF THE AVNIR-2 TOA REFLECTANCES AND THE SIMULATED AVNIR-2 TOA REFLECTANCE S

Day of year 2006	B1	B2	B3	B4
136	1.001	1.011	0.946	0.860
145	0.950	0.963	0.910	0.808
146	0.978	0.985	0.935	0.849
150	0.954	0.976	0.916	0.829
151	0.913	0.953	0.913	0.826
172	0.978	0.996	0.924	0.833
173	0.908	0.938	0.893	0.801
175	0.987	0.988	0.940	0.844
214	0.936	0.946	0.903	0.804
214	0.936	0.950	0.907	0.806
219	0.891	0.933	0.895	0.795
219	0.894	0.945	0.904	0.801
238	0.957	0.970	0.929	0.838
243	0.924	0.954	0.917	0.805
248	0.937	0.966	0.923	0.820
260	0.941	0.968	0.923	0.815
264	0.968	0.981	0.933	0.802
267	0.932	0.971	0.938	0.846
274	0.936	0.968	0.930	0.832
284	0.948	0.977	0.944	0.842
288	0.990	0.995	0.945	0.837
289	0.953	0.988	0.950	0.849
310	0.972	0.991	0.945	0.858
311	0.993	1.014	0.965	0.881
334	1.028	1.001	0.935	0.836
356	0.990	0.997	0.942	0.849
Mean ratio	0.954	0.974	0.927	0.829

C. *Conclusion*

Both spectral differences and BRDF conditions are account for in the inter calibration between MERIS and AVNIR-2. The day to day variation of the inter calibration between the two instruments is weak which make us confident in the BRDF correction. The H2O transmittance is accounted for in B4 in AVNIR.

V. CONCLUSION

This paper summarizes the radiometric calibration activities that were carried out to assess the performance of the Advanced Visible and Near Infrared Radiometer type 2 (AVNIR-2) sensor onboard the Advanced Land Observing Satellite (ALOS) platform. The assessments were achieved via three methodologies enabling comparison of AVNIR-2 to currently flying sensors over the Libyan desert, during the first year of operation.

Preliminary conclusions can be drawn concerning the results methodologies associated with the three intercomparisons.

Concerning intercomparison 1, the methodology involves calibration of surface observations based on image statistics from areas observed nearly simultaneously by the two sensors. The average percent differences in at-sensor reflectance estimates obtained from these sensors agree within seven percent. These values have been tested at one date, over somewhat peculiar target (Libya) – more dates and sites must be tested to develop more robust relationships. Additional work to characterize the artifacts and absolute calibration is in progress (challenges include atmospheric influences, ground sample distance (GSD), RSR differences, bi-directional reflectance function (BRDF), and geometric co-location)

From intercomparison 2, it appears that gaseous absorption of dioxygen and water vapour is significant in AVNIR-2 bands 2, 3, and 4 and should be taken into account when intercomparing AVNIR-2 data to narrow band sensor data. In particular, in band 4, we find that absorption amounts to about 7% on average.

In intercomparison 3, a relationship between the TOA reflectance and the scattering angle is found from which AVNIR-2 data can be simulated using the spectrally resampled MERIS data.

Table 11 is a synthesis of the comparisons of the AVNIR-2 data to the radiometric scale of other instruments, respectively, L5 TM, MERIS and again MERIS for intercomparison 1, 2, and 3.

TABLE 11: SYNTHESIS OF RESULTS

	Intercomparison1: comparison with L5 TM radiometric scale	Intercomparison2: comparison with MERIS radiometric scale	Intercomparison3: comparison with MERIS radiometric scale
Band 1	- 6.5 %	-7.0%	-4.60%
Band 2	1.2%	-1.1%	-1.4%
Band 3	Saturation	Saturation	Saturation
Band 4	-5.0 %	-3.5%	-10.30%

The results of sensor intercomparisons presented in Table 11 indicate that the radiometric calibration of AVNIR-2 is satisfactory, given the error bar of the methodologies which is estimated to be around 5 %. All results are consistent across the intercomparisons and bands but for intercomparison 1 and 2 – band 1 indicating an underestimation of ANVIR-2 in the blue part of the spectrum. Intercomparison 3 , in band 4, indicates a significant underestimation of ANVIR-2 not confirmed by other intercomparisons. This could also be explained by the water vapour correction applied, which is directly inherited from intercomparison 2 (although the AVNIR-2 data series differ between the two intercomparisons).

Intercomparison 2 appears to indicate that sufficiently long time series of AVNIR-2 data over a natural target could enable the identification of instrument degradation. The shorter the central wavelength of the band, the stronger the degradation appears to be over time: respectively 13.2 %.year-1, 8.8 %.year-1, 5.9 %.year-1 and 0.1 %.year-1 in band 1, 2, 3 and 4, with respect to the radiometric scale of MERIS. For band 3, such degradation is difficult to interpret because of saturation due to inappropriate gain settings. These degradation figures can however only be confirmed after one full year of AVNIR-2 data over the Libyan site have been acquired and processed to ensure that such degradation is not an artifact induced by the methodology and the natural annual variations of the TOA reflectance.

More AVNIR-2 data, with appropriate gain setting are needed to continue monitoring and confirm the evolution of the radiometric behavior the AVNIR-2 instrument.

ACKNOWLEDGMENT

AVNIR-2 data were provided by JAXA. MODIS and SeaWiFS data were obtained from the NASA Langley Research Center Atmospheric Sciences Data Center. AATSR and MERIS data were provided by the European Space Agency. The POLDER-3 data were provided by the Centre National d'Etudes Spatiales.

REFERENCES

[1] Bouvet M. (2006), Intercomparison of multispectral imagers over natural targets, *IGARSS 2007 proceedings*.

[2] Roujean J.-L.. Leroy M., and Deschamps P.-Y., (1992). A bidirectional reflectance model of the Earths surface for the correction of remote sensing data. Journal of Geophysica1 Research, 97(DIS), 20,455-20.468.

[3] Svetlana Y. Kotchenova, Eric F. Vermote, Raffaella Matarrese and Frank J. Klemm, Jr. Validation of a vector version of the 6S radiative transfer code for atmospheric correction of satellite data. Part I: Path radiance, Applied Optics, Vol. 54, No. 26, 10 September 2006.

[4] Thuillier, G., M. Hersé, P. C. Simon, D. Labs, H. Mandel, D. Gillotay, and T. Foujols, 2003, "The solar spectral irradiance from 200 to 2400 nm as measured by the SOLSPEC spectrometer from the ATLAS 1-2-3 and EURECA missions, *Solar Physics*, 214(1): 1-2